

EPR and Luminescence of F^+ Centers in Bulk and Nanophosphor Oxyorthosilicates

D. Wayne Cooke, Michael W. Blair, James F. Smith, Bryan L. Bennett, Luiz G. Jacobsohn, Edward A. McKigney, and Ross E. Muenchausen

Abstract—The main thermally stimulated luminescence glow peak in irradiated oxyorthosilicates occurs near 360–400 K and has been postulated to comprise an electron trapped at an oxygen vacancy (F^+ center). We have used electron paramagnetic resonance spectroscopy to identify this defect in $\text{Ln}_2\text{SiO}_5 : \text{Ce}$ ($\text{Ln} = \text{Lu}$ and Y) and show that it consists of a single electron trapped at a non-silicon-bonded oxygen vacancy in both bulk and nanophosphor oxyorthosilicates. Both Lu- and Y-based nanophosphors form seven- and nine-oxygen coordinated structures ($P2_1/c$) whereas the bulk phosphors form six- and seven-oxygen coordinated structures ($C2/c$). In each case the F^+ center predominately forms at the larger oxygen site. A typical resonance comprises a single Gaussian line broadened by hyperfine interaction with g-values near the free electron value and hyperfine coupling ~ 0.4 mT. The F^+ center can be annealed and radiation-induced, consistent with the thermally stimulated luminescence glow peak behavior.

Index Terms—Electron paramagnetic resonance, F^+ center, luminescence, oxyorthosilicates.

I. INTRODUCTION

INTEREST in optical properties of cerium-doped oxyorthosilicates, $\text{Lu}_2\text{SiO}_5 : \text{Ce}$ (LSO) and $\text{Y}_2\text{SiO}_5 : \text{Ce}$ (YSO) primarily stem from their application to radiation detection, especially medical imaging [1]. More recently, they have been synthesized as nanophosphors and examined to assess the effects of reduced dimensionality on their structural and optical properties [2]. Thermally stimulated luminescence (TSL) measurements of oxyorthosilicates show the presence of intrinsic traps with a major glow peak near 360–400 K. Although the origin of this peak has not been established, it has been speculated that it comprises an electron trapped at an oxygen vacancy of the host lattice [3]. The previous work examined only bulk oxyorthosilicates and luminescence studies to identify oxygen vacancies, but the present study aims to examine the nature of the TSL peak in both bulk and nanophosphor oxyorthosilicates using two different techniques.

We have used electron paramagnetic resonance (EPR) spectroscopy to examine both bulk and nanophosphor LSO and YSO and have identified the signal associated with an electron

trapped at an oxygen vacancy (F^+ center). It is characterized by Zeeman and hyperfine interactions with typical g-values near the free electron value and hyperfine coupling ~ 0.4 mT. The F^+ center can be radiation induced and annealed, consistent with thermal annealing of the TSL glow peak. In addition, we have examined the Ce^{3+} resonances in both bulk and nanophosphor LSO and YSO and found shifts in g-values as well as inhomogeneous broadening of the resonance line due to lattice disorder.

II. EXPERIMENTAL ASPECTS

A. EPR

EPR measurements were made both at room temperature and liquid helium temperature with a Bruker EleXsys E-500 spectrometer equipped with an Oxford cryostat. The X-band spectrometer consists of an SHQE-W1 cavity, SuperX bridge, NMR Tesla meter, and field/frequency stabilizer. Data were acquired by taking the first derivative of the absorption curve with field modulation 100 kHz and amplitude 0.4 mT. Typical microwave power applied to the sample was 5 mW, although in some cases it was increased to 10 mW. Powder samples were placed in a fused silica tube and inserted into the microwave cavity for measurement.

B. TSL

Thermally stimulated luminescence glow curves were obtained with a commercial reader capable of uniformly heating the sample between 300 and 600 K. In a typical experiment the sample, in powder form, was exposed to 25 keV X-rays at room temperature then placed on a silver planchet and heated to 600 K in the presence of flowing N_2 . A uniform heating rate of 5 K/s was used and the data were fitted to the usual Randall-Wilkins expression relating TSL intensity to temperature, thermal activation energy, frequency factor, and order of kinetics [4].

C. Samples

Bulk samples of LSO and YSO were obtained by grinding single crystal specimens that had been grown by the Czochralski method to $< 40 - \mu\text{m}$ particle size with a mortar and pestle. X-ray diffraction confirmed phase purity and monoclinic structure with $C2/c$ space group. The small distribution coefficient for Ce in LSO and YSO (0.22) is the limiting factor for the Ce concentration, and the Ce concentration is approximately 0.055 at.% relative to Lu or Y. This structure is comprised of SiO_4 tetrahedra with four different oxygen ions and one non-Si-

Manuscript received June 13, 2007; revised September 27, 2007. This work was supported by the U.S. Department of Energy Office of Basic Energy Sciences under Grant number 09SCPE972.

The authors are with the Los Alamos National Laboratory, Los Alamos, NM 87545 USA (e-mail: cooke@lanl.gov; mblair@lanl.gov; jf-smith@lanl.gov; blbennett@lanl.gov; lgjacob@lanl.gov; mckigney@lanl.gov; rossm@lanl.gov).

Digital Object Identifier 10.1109/TNS.2008.922798

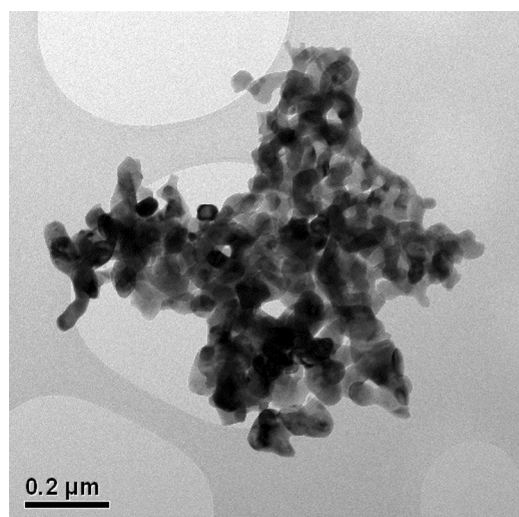


Fig. 1. TEM of nanophosphor YSO showing micron size agglomerated crystallites.

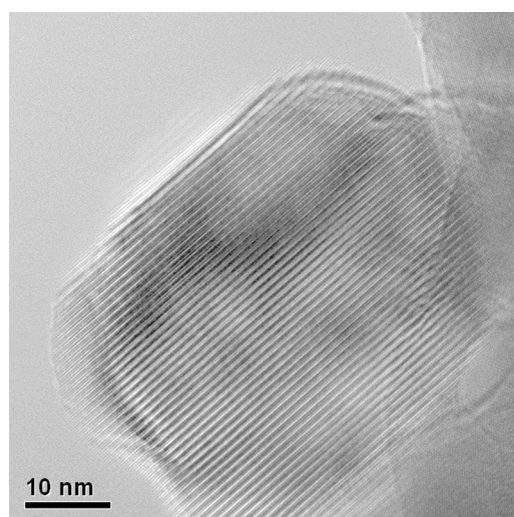


Fig. 2. TEM of nanophosphor YSO showing individual crystallite.

bonded oxygen that is surrounded by four Lu (Y) ions [5]. Lu (Y) ions occupy two crystallographic sites coordinated with either six or seven oxygen ions. For the six-oxygen coordinated site in LSO, the Lu-O distances vary from 2.16 to 2.24 Å; the Lu-O distances for the seven-oxygen site vary from 2.16 to 2.34 Å, with the seventh oxygen at 2.61 Å [6].

Nanophosphor LSO and YSO were prepared by the glycine-nitrate solution combustion technique [7]. These specimens form a monoclinic structure with $P2_1/c$ space group whereby the Lu (Y) ions occupy two crystallographic sites coordinated with either seven or nine oxygen ions, in contrast to the $C2/c$ structure of bulk samples. Cerium concentration of the nanophosphors is ~ 1.0 at.%. Energy dispersive x-ray analysis (EDX) with scanning transmission electron microscopy (STEM) found that the dopant concentration was uniform in the samples (Muenchausen *et al.*, these proceedings). For the seven-oxygen coordinated site in bulk YSO, the Y-O distances vary from 2.23 to 2.56 Å, and for the nine-oxygen site the distances vary from 2.20 to 2.95 Å [8]. Presumably, these distances are similar in nanophosphor specimens, but this has not been verified.

X-ray diffraction data confirmed the structure and phase purity of these specimens and TEM showed micron sized particles of agglomerated crystallites (Fig. 1) with average crystallite size ~ 30 nm, as shown in Fig. 2. The crystallite size has also been confirmed by Sherrer analysis of the XRD data [13].

III. RESULTS AND DISCUSSION

A. EPR

In Ce-doped LSO and YSO, the larger Ce^{3+} ion (1.034 Å) replaces the Y^{3+} (0.893 Å) or Lu^{3+} ion (0.848 Å). Free Ce^{3+} ion has a $4f^1$ configuration with ground state $^2F_{5/2}$ and is paramagnetic. On the other hand, Lu^{3+} and Y^{3+} possess closed shell configurations and are diamagnetic. In LSO and YSO the Ce^{3+} ground state is split into three degenerate levels comprising Kramers doublets [6]. Owing to lifetime broadening the

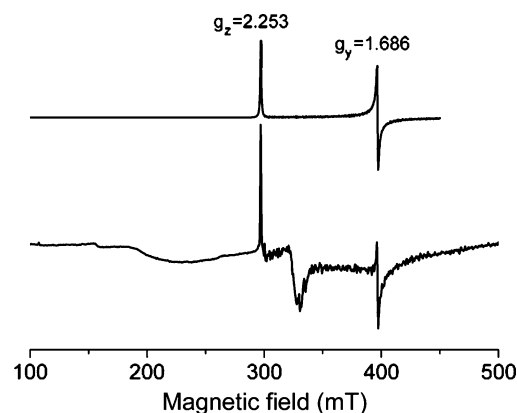


Fig. 3. EPR spectrum of bulk LSO taken at 6 K (lower curve) and simulated spectrum assuming only electronic Zeeman interaction (upper curve).

Ce^{3+} resonances are only observed for temperatures less than ~ 50 K.

The lower curve of Fig. 3 shows the EPR spectrum of bulk LSO taken at 6 K. The two sharp resonances are due to Ce^{3+} and are in agreement with data of [9]. They are assigned to the larger (seven-oxygen coordinated) substitutional site, denoted Ce_I [6]. Because Ce has no nuclear moment there is no hyperfine interaction of the unpaired electron spin and nucleus. The spectrum is readily described solely by a spin Hamiltonian that includes only the electronic Zeeman interaction

$$\hat{H} = g\beta HS \quad (1)$$

with spectroscopic splitting factor g , Bohr magneton β , magnetic field H , and electron spin S . The simulated spectrum is shown by the upper curve of Fig. 3. The additional resonance occurring near 330 mT is attributed to an F^+ center, which will be discussed later.

The lower curve of Fig. 4 shows the corresponding EPR spectrum of nanophosphor LSO with the simulated spectrum shown by the upper curve. The main difference between bulk and nanophosphor Ce_I resonances is the enhanced broadening

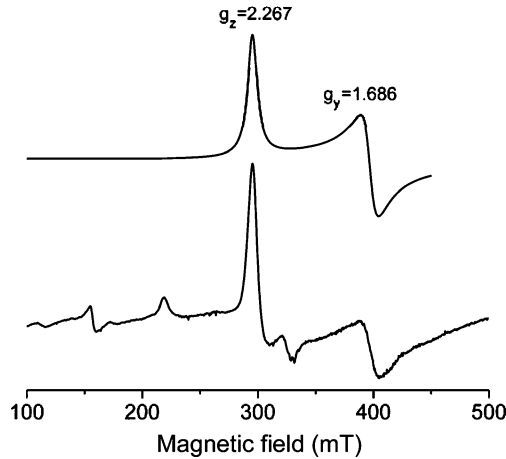


Fig. 4. EPR spectrum of nanophosphor LSO taken at 4 K (lower curve) and simulated spectrum assuming only Zeeman interaction of Ce^{3+} ions (upper curve). Resonance near 150 mT is Tb impurity. 220 mT signal is attributed to Ce_{II} and resonance near 310 mT is F^+ center.

TABLE I
 Ce^{3+} EPR PARAMETERS

Phosphor	g_y	g_x
LSO Bulk	1.686	2.253
LSO Nano	1.686	2.267
LSO Bulk ^a	1.698	2.264
YSO Bulk	1.610	2.348
YSO Nano	1.500	2.266

^a[9]

of the nanophosphor line width. This is attributed to a distribution of g -values presumably associated with lattice disorder. A comparison of g -values for all Ce_{I} resonances is given in Table I. Note that we have used results obtained in [6] to assign individual g -components in our powder specimens.

Two additional low field resonances are readily observed in nanophosphor LSO. One near 150 mT is attributed to Tb impurity and one near 220 mT is tentatively associated with Ce^{3+} in the smaller seven-oxygen coordinated site, which we denote Ce_{II} [6]. Recall that nanophosphor LSO and YSO form the $\text{P2}_1/\text{c}$ structure with seven- and nine-oxygen coordination as opposed to six- and seven-oxygen coordination of the bulk phosphor.

The lower curve of Fig. 5 shows the EPR spectrum of bulk YSO and the upper curve shows the simulated spectrum. The prominent Ce_{I} resonances are well resolved and adequately described by the Zeeman interaction of the unpaired spin with the magnetic field, (1). These spectra may be compared to nanophosphor YSO shown in Fig. 6. Shift in g -values of bulk and nanophosphor YSO are larger than those observed in LSO (see Table I) and there is considerable broadening of the Ce^{3+} resonances due to lattice disorder. The resonance near 150 mT can be assigned to Tb impurities based upon EPR spectra of Y_2O_3 doped with Tb (not shown). The spectrum also shows the Ce_{II} resonance near 220 mT and the F^+ center resonance near 330 mT.

We now discuss the F^+ center resonance that is observed in bulk and nanophosphor LSO and YSO. For illustrative purposes

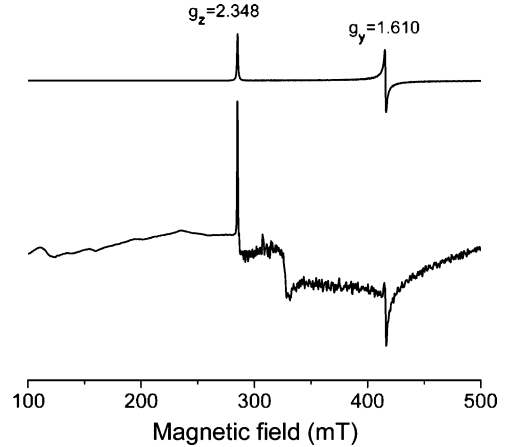


Fig. 5. EPR spectrum of bulk YSO taken at 9 K (lower curve) and simulated spectrum assuming only Zeeman interaction (upper curve).

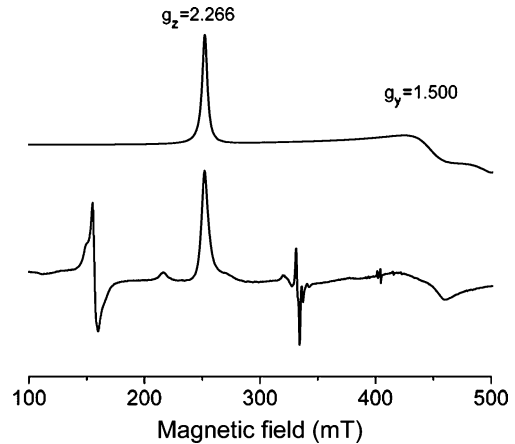


Fig. 6. EPR spectrum of nanophosphor YSO taken at 10 K (lower curve) and simulated spectrum assuming only Zeeman interaction of Ce^{3+} ions. Resonance near 150 mT is due to Tb impurity. Resonance near 220 mT is attributed to Ce_{II} and signal near 330 mT is associated with F^+ center.

we show in Fig. 7 the F^+ center resonance in bulk YSO obtained at 300 K after 60 minutes of exposure to 25 keV X-rays at room temperature; (a) is the experimental spectrum, (b) is the simulated spectrum where hyperfine interaction with the ^{89}Y nucleus is included, and (c) is the simulated spectrum absent hyperfine interaction. This defect comprises a single electron trapped at an oxygen vacancy in the host lattice. In the bulk phosphor it occupies the non-Si-bonded oxygen vacancy of the larger site, i.e., the seven-oxygen coordinated site. Similarly, in nanophosphors it occupies the non-Si-bonded oxygen vacancy of the nine-coordinated site. In either case the oxygen vacancy is coordinated with four Y ions (four Lu ions in LSO). For comparison, Fig. 8 shows the EPR spectrum of nanophosphor YSO. Similar results (not shown) were obtained for bulk and nanophosphor LSO. The F^+ center is observed over the full experimental temperature range 4–300 K.

A single electron in an oxygen vacancy (F^+ center) is paramagnetic and is expected to yield a single resonance centered near the free electron g -value (2.0023) [9]. This is consistent with our results where the F^+ center g -values for bulk and nanophosphor LSO and YSO vary between 2.004 and 2.006.

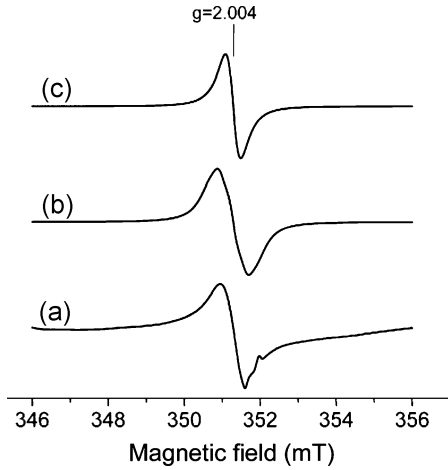


Fig. 7. EPR spectra of the F^+ center in bulk YSO obtained at 300 K after 60 minutes of X-ray exposure. (a) Experimental spectrum; (b) simulated spectrum that includes hyperfine interaction with ^{89}Y nuclei; and (c) simulated spectrum absent hyperfine interaction.

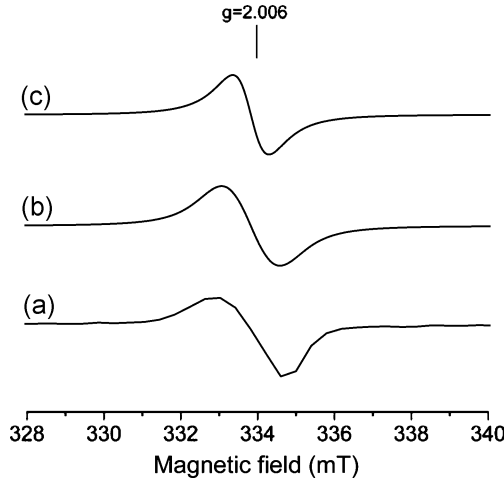


Fig. 8. EPR spectra of the F^+ center in nanophosphor YSO obtained at 300 K after 60 minutes of X-ray exposure. (a) Experimental spectrum; (b) simulated spectrum that includes hyperfine interaction with ^{89}Y nuclei; and (c) simulated spectrum absent hyperfine interaction.

In each case the F^+ center resonance lineshape is Gaussian rather than Lorentzian, suggesting the presence of hyperfine coupling. The best result is obtained when the data are fitted with a spin Hamiltonian that includes electron Zeeman and hyperfine interactions

$$\tilde{H} = g\beta HS + a \vec{S} \cdot \vec{I} \quad (2)$$

with nuclear spin I , and hyperfine coupling constant a . For powder specimens the data are fitted with an isotropic coupling constant. Figs. 8(b) and 9(b) show that the best fits to the data are obtained by including the hyperfine interaction [compare with spectra in Figs. 8(c) and 9(c)]. The magnitude of a in bulk and nanophosphor YSO is 0.28 and 0.43 mT, respectively; corresponding values for LSO are 0.45 and 0.43 mT, respectively. The hyperfine interaction arises from the interaction of the F^+ center electron with the four near neighbor ^{89}Y nuclei ($I = 1/2$; natural abundance = 100%) in YSO or the four near neighbor ^{175}Lu nuclei ($I = 7/2$; natural abundance = 97%) in LSO.

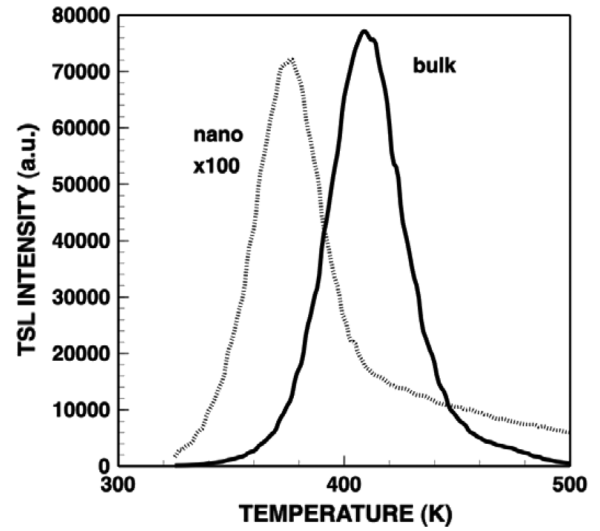


Fig. 9. TSL glow curves of bulk and nanophosphor YSO. Note the scale change for the nanophosphor curve.

Fundamentally, a is the Fermi contact term, which is proportional to the squared amplitude of the electronic wave function at the nucleus [10]. Because p , d , and f orbitals have nodes at the nucleus the electron must have some s -orbital character, which is expected from an F^+ center and is consistent with the present data.

It is interesting to compare hyperfine coupling constants for the F^+ center in bulk LSO and YSO. Lu-O distances are smaller (2.16–2.34 Å) than Y-O distances (2.20–2.95 Å); consequently, we expect the magnitude of a to reflect this difference, even assuming lattice relaxation around the oxygen vacancy. Indeed, a is smaller in bulk YSO (0.28 mT) than in LSO (0.45 mT). As dimensionality is reduced to form the nanophosphor, a for LSO remains essentially unchanged (0.43 mT), but increases significantly in YSO (0.43 mT), suggesting that the lattice has contracted around the oxygen vacancy. This unusual behavior of Y is also manifested in the g -value shifts of the Ce_I resonances. There is very little shift in these values between bulk and nanophosphor LSO whereas YSO shows a large shift. This unusual behavior of Y is not understood.

B. TSL

Fig. 9 shows the TSL glow curves for bulk and nanophosphor YSO after 15 s of 25 keV X-ray exposure. Similar data were obtained for LSO. Randall-Wilkins analysis of the glow curves yields a thermal activation energy of 1.12 eV for bulk YSO and 0.93 eV for nanophosphor YSO. Because of the different densities of the two specimens, the data are normalized to mass. We suggest that these two glow peaks arise from thermal release of the F^+ center electrons in bulk and nanophosphor YSO as has been seen previously [11], [12]. Differences in the glow peak maxima are due to slightly different thermal binding energies of the electrons due to different oxygen coordination. As indicated in Fig. 9, the YSO bulk phosphor glow curve near 400 K is approximately two-orders-of-magnitude greater than the nanophosphor glow curve (peak near 360 K). This implies a larger concentration of oxygen vacancies in the bulk

material. The solution combustion method used to fabricate the nanophosphor is oxygen rich, whereas the Czochralski method is relatively oxygen deficient. Thus, we expect a larger concentration of oxygen vacancies in the latter specimen. Preliminary measurements of the spin concentration, as extracted from EPR measurements, are in agreement with this conclusion. Moreover, initial annealing and irradiation experiments show that the F^+ center observed by EPR can be thermally annealed at 400 K and can also be induced by x irradiation. Experiments to quantify this correlation are in progress.

IV. CONCLUSION

We have used EPR to identify the F^+ center in bulk and nanophosphor LSO and YSO. This defect comprises a single electron trapped at the non-Si-bonded oxygen vacancy of the host lattice. For the six- and seven-oxygen coordinated sites of the bulk phosphors, the electron is trapped primarily at the larger seven-oxygen coordinated site. Similarly, for the nanophosphors, the electron is trapped at the nine-oxygen coordinated site of the non-Si-bonded oxygen vacancy. These F^+ centers are associated with TSL glow peaks near 360–400 K in the respective phosphors. Bulk and nanophosphor LSO show nearly identical hyperfine coupling between the Lu ions and the F^+ center electron. Conversely, nanophosphor YSO shows a significant increase in a relative to the bulk value, indicative of lattice contraction around the oxygen vacancy.

Ce^{3+} resonances were also observed in these materials and the results demonstrate broadening of the EPR linewidth consistent with a distribution of g -values due to lattice disorder. Ce_{I} g -values in LSO are not significantly affected as physical size is reduced to nanoscale dimensions whereas YSO exhibits relatively large g -value shifts.

REFERENCES

- [1] P. Dorenbos, "Light output and energy resolution of Ce^{3+} -doped scintillators," *Nucl. Instrum. Meth. Phys. Res. A*, vol. 486, pp. 208–213, Jun. 2002.
- [2] D. W. Cooke, J.-K. Lee, B. L. Bennett, J. R. Groves, L. G. Jacobsohn, E. A. McKigney, R. E. Muenchausen, M. Nastasi, K. E. Sickafus, M. Tang, J. A. Valdez, J.-Y. Kim, and K. S. Hong, "Luminescent properties and reduced dimensional behavior of hydrothermally prepared $Y_2SiO_5 : Ce$ nanophosphors," *Appl. Phys. Lett.*, vol. 88, pp. 103108-1–103108-3, Mar. 2006.
- [3] D. W. Cooke, B. L. Bennett, R. E. Muenchausen, K. J. McClellan, J. M. Roper, and M. T. Whittaker, "Intrinsic trapping sites in rare-earth and yttrium oxyorthosilicates," *J. Appl. Phys.*, vol. 86, pp. 5308–5310, Nov. 1999.
- [4] D. W. Cooke, B. L. Bennett, K. J. McClellan, J. M. Roper, and M. T. Whittaker, "Similarities in glow peak positions and kinetics parameters of oxyorthosilicates: Evidence for unique intrinsic trapping sites," *J. Lumin.*, vol. 92, pp. 83–89, Dec. 2000.
- [5] J. Felsche, "The crystal chemistry of the rare-earth silicates," in *Structure and Bonding*, J. Dunitz, P. Hemmerich, J. Ibers, C. Jorgensen, J. Neilands, R. Nyholm, D. Reiner, and R. Williams, Eds. Berlin, Germany: Springer-Verlag, 1973, vol. 13, pp. 99–197.
- [6] L. Pidol, O. Guillot-Noël, A. Kahn-Harari, B. Viana, D. Pelenc, and D. Gourier, "EPR study of Ce^{3+} ions in lutetium silicate scintillators $Lu_2Si_2O_7$ and Lu_2SiO_5 ," *J. Phys. Chem. Solids*, vol. 67, pp. 643–650, Apr. 2006.
- [7] J. J. Kingsley and K. C. Patil, "A novel combustion process for the synthesis of fine particle α -alumina and related oxide materials," *Mater. Lett.*, vol. 6, pp. 427–432, Jul. 1988.
- [8] J. Wang, S. Tian, G. Li, F. Liao, and X. Jing, "Preparation and X-ray characterization of low-temperature phases of R_2SiO_5 (R = rare earth elements)," *Mater. Res. Bull.*, vol. 36, pp. 1855–1861, Jul. 2001.
- [9] B. Henderson and A. K. Garrison, "Hyperfine interaction of defects in insulators," *Adv. Phys.*, vol. 22, pp. 423–528, Jul. 1973.
- [10] A. Carrington and A. McLachlan, *Introduction to Magnetic Resonance*. New York: Harper & Row, 1967, ch. 2.
- [11] A. Meijerink, W. J. Schipper, and G. Blasse, "Photostimulated luminescence and thermally stimulated luminescence of Y_2SiO_5 -Ce,Sm," *J. Phys. D: Appl. Phys.*, vol. 24, pp. 997–1002, Feb. 1991.
- [12] R. Visser, C. L. Melcher, J. S. Schweitzer, H. Suzukia, and T. A. Tombrello, "Photostimulated luminescence and thermoluminescence of LSO scintillators," *IEEE Trans. Nucl. Sci.*, vol. 41, no. 4, pp. 689–693, Aug. 1994.
- [13] B. D. Cullity, *Elements of X-Ray Diffraction*. Reading, MA: Addison-Wesley, 1956, ch. 3.